Fluid-dynamic and thermo-mechanical analyses of the ITER Electron Cyclotron Miter Bend mirror for the off-centered beam scenario

Avelino Mas Sánchez[a*], Thierry Boutboul[b], René Chavan[a], Davide Dall'Acqua[b], Timothy Goodman[a], Cinta Marraco Borderas[a], Humberto Torreblanca Quiroz[a], Anastasia Xydou[a]

[a] *Ecole Polytechnique Fédérale de Lausanne (EPFL), Swiss Plasma Center (SPC), CH-1015 Lausanne, Switzerland*
[b] *Fusion for Energy, Josep Pla 2, Torres Diagonal Litoral B3, E-08019 Barcelona, Spain*

The Electron Cyclotron Upper Launcher (EC UL) is an eight-beamline ITER antenna that will be used to counteract magneto-hydrodynamic plasma instabilities by aiming mm-wave power at 170 GHz. The primary vacuum boundary at the port plug extends into the port cell region through the ex-vessel mm-wave waveguide components, defining the so-called First Confinement System (FCS). Each FCS beamline, designed for the transmission of up to 1.08 MW, is delimited by the closure plate at the port plug back-end and by a diamond window in the port cell. The FCS essentially consists of a Z-shaped set of straight corrugated waveguides connected by Miter Bends (MB) with a nominal inner diameter of 50 mm.

Recent tests at the FALCON facility have shown that the ohmic losses deposited on the MB mirror reflecting surface during the beam transmission do not follow the pure HE_{11} theoretical distribution given by a perfectly-centered Bessel heat flux profile. For this reason, the MB mirror cooling design has been modified to a three-channel spiral-shaped configuration, which is able to better cope with possible beam offsets. This paper reports the status of the MB mirror as well as the fluid-dynamic and thermo-mechanical analyses carried out to validate this design.

Keywords: ITER; ECH; Upper Launcher; Miter Bend; Waveguides

1. Introduction

The ITER Electron Cyclotron (EC) system consists of 24 gyrotrons providing up to 20 MW of mm-wave power at 170 GHz with transmission lines connecting the gyrotrons with an Equatorial Launcher (EL) and four Upper Launchers (UL, [1]). The main function of the ULs is to stabilize the neoclassical tearing modes (NTM) for q=3/2 and q=2/1, where assessment of stabilization criteria defines a maximum beam width at the island position and a conservative minimum power deposition, both mainly depending on the plasma safety factor q and the toroidal injection angle β.

The mm-wave components in the eight beamlines of each EC UL are divided into essentially quasi-optical in-vessel and guided-wave ex-vessel assemblies. The ex-vessel waveguide components, extending the primary vacuum boundary of the port plug into the port cell region on both sides of the bio-shield wall, are part of the First Confinement System (FCS, Fig. 1), for which, the ITER SIC-1 requirements apply.

author's email: avelino.massanchez@epfl.ch

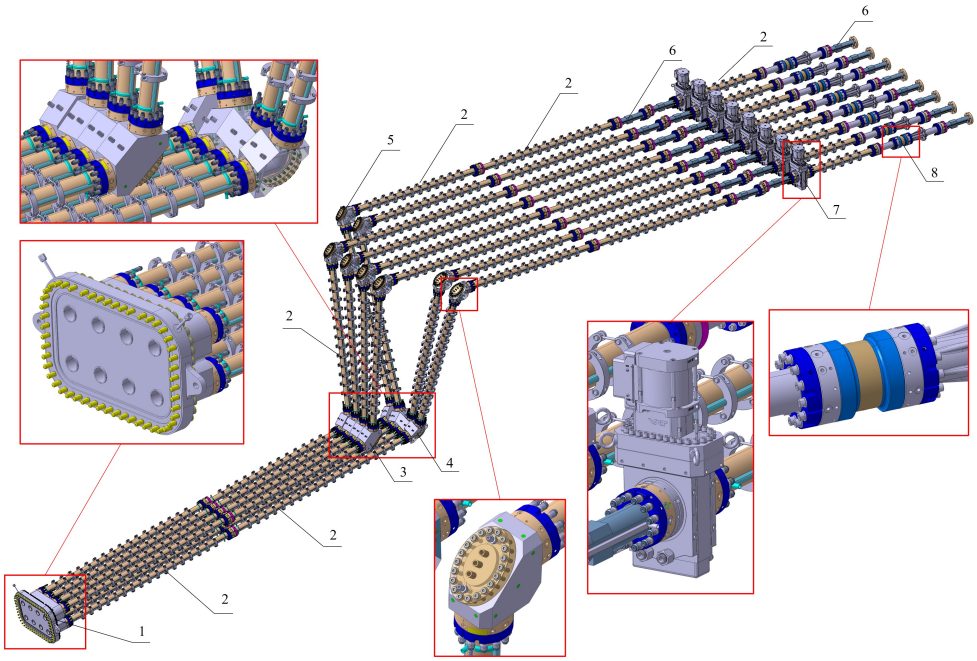

Fig. 1. Current state of the Fist Confinement System. 1. Closure plate sub-plate, 2. Standard WGs, 3. Upper MBMB, 4. Lower MBMB, 5. MBs, 6. Clamped WGs, 7. Isolation valves, 8. Diamond windows

The FCS is made of a set of CuCr1Zr corrugated waveguides (WGs) with a nominal inner and outer diameter of 50 mm and 66 mm, respectively. This system is delimited by the Closure Plate Sub-plate at the port-plug back-end with WG feedthroughs and by Diamond Window Units (DWU) located in the port cell region beyond the bio-shield (an intermediate Isolation Valve provides the double containment). Each beamline consists of straight waveguides with a quasi-vertical Z-shaped configuration connected by independent Miter Bends (MBs) at an upper location and by Monoblock Miter bends (MBMBs) at a lower location. The waveguide layout changes from horizontal plane of 1 x 8 to a 2 x 4 WG configuration at the MBMBs for entry into the torus.

2. Design description

The Miter Bends (Fig. 2) are the components that connect two pieces of WG to form an angle different than 0° between their axes (90° for the single MBs and around 100° for MBMBs). The Miter Bend mainly consists of a MB body with two corrugated feedthroughs (defining the required angle) and a MB mirror attached to it by bolted connection The alloy CuCr1Zr was selected as the material for most of these two components due to its high strength and high thermal conductivity, which minimizes the ohmic losses and improves the heat dissipation during mm-wave power transmission.

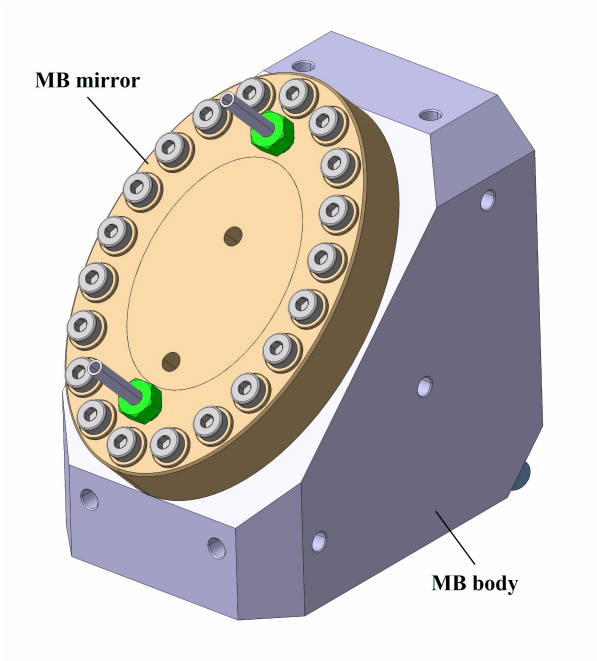

Fig. 2. Current design of the ITER EC Miter Bend

The MB mirror (Fig. 3) is the component dedicated to reflecting the mm-wave beam allowing its propagation through the FCS. This component consists in an elliptical CuCr1Zr plate of 28 mm thickness, which is bolted to the MB body through 20 M8 bolts. To comply with ITER SIC-1 requirements, this mechanical coupling shall contain two concentric metallic seals with two leak monitoring ports between the seals.

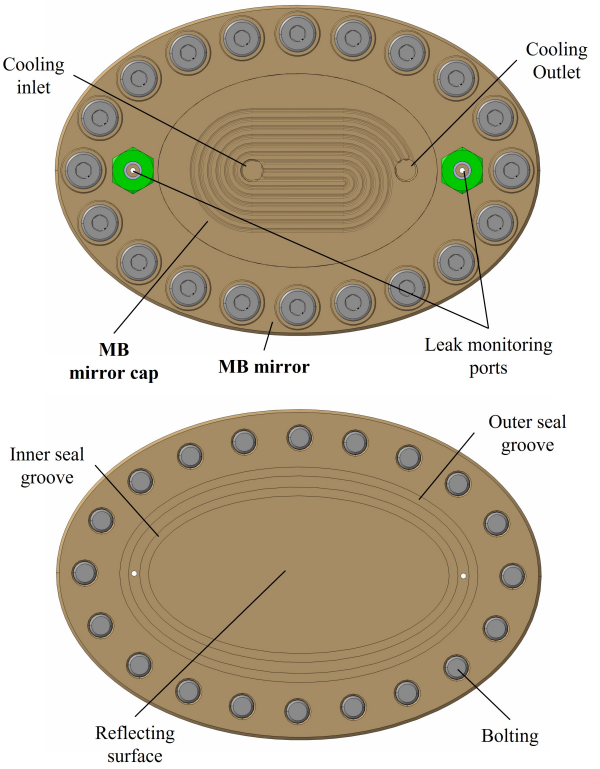

Fig. 3. Non-reflecting (top) and reflecting sides (bottom) of the MB mirror

During the beam reflection, part of the power is deposited on the reflecting surface due to the ohmic losses. This requires the implementation of a high-efficient cooling design capable to dissipate this power so that the mirror temperature and associated thermal deformation can be maintained within acceptable limits.

For previous cooling concepts, the water reached the MB mirror through the inlet located at the center, which impinges on the mirror reflecting surface. The intrinsic problem associated to this concept lies in the flow recirculation taking place at the jet impingement location, which produced very low velocity values and therefore, a very low heat transfer at this location [2]. Therefore, this concept was replaced by a cooling design consisting of a spiral-shaped circuit with one inlet and one outlet. In this circuit, the inlet is shifted the mirror center to obtain a completely developed flow at the heat flux peak location [3].

Recent experimental tests at the FALCON facility have shown that the beam losses deposited on the MB mirror reflecting surface during the beam transmission are not fully represented by the theoretical distribution of a perfectly-centered heat flux Bessel function. Instead, these tests showed a deviation of the beam center and an increase of the peak power density [4]. For this reason, the MB mirror cooling design was modified to a three-channel configuration, which can dissipate more uniformly the deposited power and therefore, is less dependent on possible beam offsets.

A rectangular cross-section of 1.5 mm width and 10 mm height is considered for the cooling channels, the distance between channels is also chosen as 1.5 mm. The minimum reflecting surface thickness (distance between the cooling water and the surface where the power is deposited) is chosen as 3 mm, which is a good compromise between maximizing the cooling efficiency and reliably containing the coolant pressure.

The cooling channels will be machined from the CuCr1Zr plate by electrical discharge machining. Then, these channels shall be covered with the MB mirror cap welded by diffusion bonding. The MB mirror cap is defined to be made in stainless steel 316L(N)-IG since performing the diffusion bonding between this material and CuCr1Zr is less challenging than between two pieces made in CuCr1Zr. Since the 316L(N)-IG MB mirror cap is far from the heat source the use of this material does not reduce the cooling performance.

3. Fluid-dynamic analyses

A steady-state fluid-dynamic simulation is performed in ANSYS Workbench 2021 R2 CFX [5] to assess the flow distribution and heat transfer taking place in the ECH MB mirror during the mm-wave normal operation for the beam power of 1.08 MW [6]. The temperature distribution obtained in this analysis is later used as an input in the coupled thermo-mechanical analysis.

3.1 Model description

3.1.1 Geometry and mesh

Due to the absence of a well-defined thermal conductance value at the coupling between the MB mirror and MB body, only the MB mirror is included in this simulation. This approach is conservative since the heat flux transferred from the MB mirror to the MB body, occurring for the assigned mass flow rates, is then not modelled in this analysis (the power deposited on the MB mirror is much larger than the one deposited in the MB body [7]). Other components, which are not so relevant for the thermal performance of the assembly, such as the bolting (bolts and washers) or the leak monitoring ports were not considered in the simulation. Two pieces of pipes are added at the cooling inlet and outlet to avoid inverse flow at these locations.

The numerical mesh (Fig. 4) consists of three non-conformal tetrahedral grids relative to the MB mirror, MB mirror cap and the cooling water with several layers of prism elements at near-wall fluid boundaries. A value of the first layer thickness of 10^{-6} m and a total

number of layers of 25 are considered for the MB mirror cooling. This size of the first layer leads to a y^+ value that is smaller than 1 on the fluid boundaries to obtain the proper resolution of the viscous sub-layer. The total number of nodes and elements for the entire model are 1885317 and 4748611, respectively.

3.1.2 Material properties and turbulence model

The material properties related to the CuCr1Zr alloy and stainless steel 316L(N)-IG are extracted from the ITER Materials Properties Handbook [8] and applied to both MB mirror and MB mirror cap, respectively. These properties are introduced in the model as temperature-dependent quantities.

For the case of the cooling water, the material properties are directly obtained from the IAPWS library available in ANSYS CFX. In this case, the properties are introduced in the model as pressure-dependent and temperature-dependent quantities. The turbulence model selected for this analysis is the Shear Stress Transport since as this model usually provides good results for cases in which there is a high heat transfer between the solid and the cooling fluid.

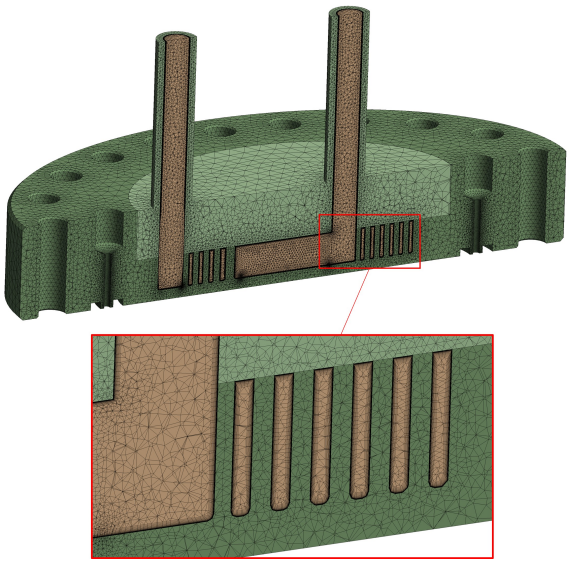

Fig. 4. Cross-section of the numerical mesh used in the fluid-dynamic analysis

3.1.3 Boundary conditions and loads

The inlet water cooling conditions of 34°C and 1 MPa provided by the ITER CCWS-1 (cooling system dedicated to the ex-vessel components) were considered for the fluid-dynamic analyses of the MB mirror [6]. The mass flow rate assigned to this component is 0.15 kg/s.

The incident power distribution (P_I) obtained in the low-power tests carried out in FALCON was scaled for the ITER beam power of 1.08 MW (Fig. 5).

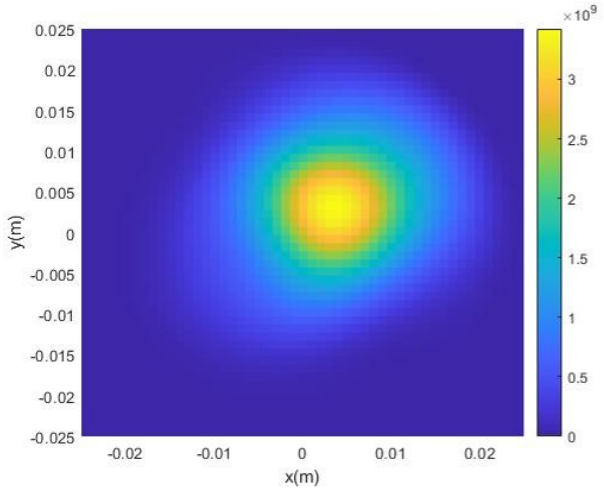

Fig. 5. Scaled incident power distribution (values in W/m²)

A fraction of the beam power will be lost on the mirror surface during the beam propagation. The fractional loss power can be calculated for each beam according to the following equation (worst-case polarization):

$$f_\Omega = 4S\sqrt{\frac{\pi\rho_e}{\lambda Z_0}}\left(\frac{1}{\cos\frac{\theta}{2}}\right) \quad (1)$$

Where ρ_e is the electrical resistivity of the CuCr1Zr [8] at 200°C, S is an enhancement factor of absorption on mirrors due to surface roughness and other imperfections (S=1.5 for MB mirrors [7]), λ is the wavelength for 170 GHz (0.00176 m), Z_0 is the impedance of free space (~120 π) and θ is the full reflection angle (90º).

The absorbed power on the MB mirrors can be calculated as:

$$q(r) = P_I \cdot f_\Omega \cdot \cos\frac{\theta}{2} \quad (2)$$

Where P_I is the incident power distribution (Fig. 5), f_Ω is the fractional loss power and θ is the full reflection angle (90º).

Eq. (2) produces a heat flux distribution on the MB mirror reflecting surface reaching a maximum value of 8.18 MW/m² (Fig. 6), which is applied to the fluid-dynamic analyses. This heat flux distribution is more pronounced than the theoretical one (producing a higher peak value) and shifted from the mirror center [3]. The total power absorbed by the MB mirror reflecting surface is 3670 W.

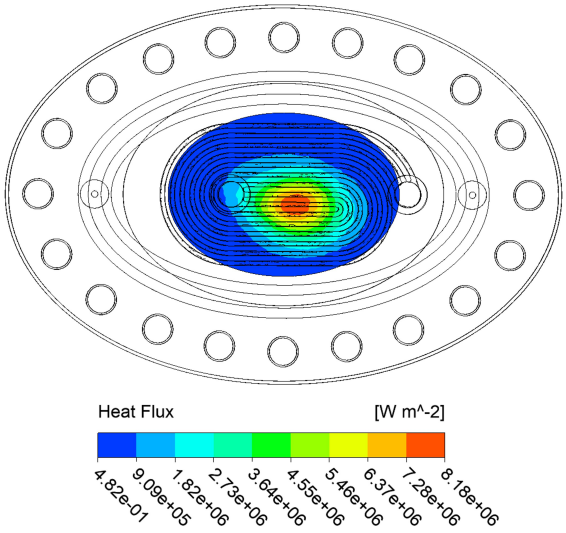

Fig. 6. Heat flux distribution on the MB mirror reflecting surface (non-reflecting side view)

3.2 Results

3.2.1 Pressure drop and flow velocity

The flow velocity reaches maximum values of up to 6.2 m/s along the central channel (Fig. 7). Low-velocity values appear at the transition between the inlet and outlet pipes and the MB mirror cooling channels, which produce a reduction of the heat transfer at these locations. However, the MB mirror is designed so that these locations are far enough from the heat flux peaks, even considering the expected off-centered beam configurations. The irradiation induced oxidation-reduction water chemistry conditions that contribute to an accelerated corrosion for the in-vessel components are not expected for the MB mirror (ex-vessel components), so no corrosion issues are expected to occur in this component.

The pressure-drop value taking place through the entire circuit is 0.036 MPa. This value is much smaller than the maximum allowable pressure drop for the CCWS-1 circuit (0.55 MPa [6]), what provides the possibility of using a single circuit to cool the MB mirrors in series with other ex-vessel components.

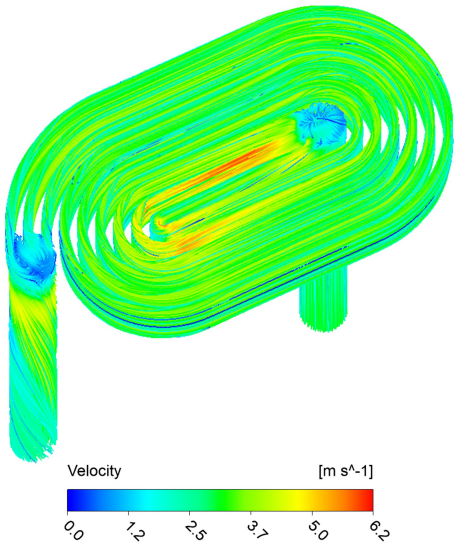

Fig. 7. Flow velocity distribution in the MB mirror

3.2.2 Temperature distribution

The maximum temperature values for the MB mirror take place at the beam center (location of the highest power density), reaching a maximum value of 174.6ºC (Fig. 8).

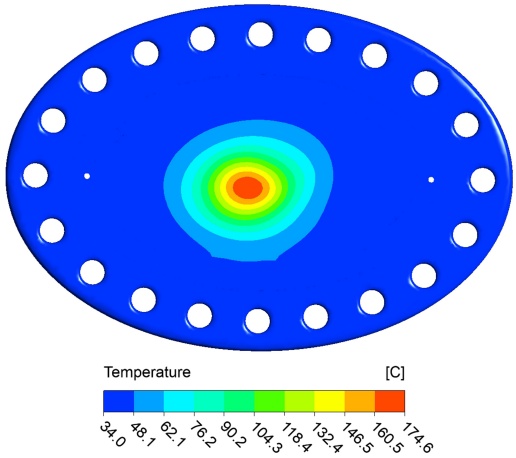

Fig. 8. Temperature distribution in the MB mirror (reflecting side view)

Regarding the cooling water, the maximum local temperature occurs at the region close to the reflecting surface, reaching 119.2ºC (Fig. 9). The boiling temperature at 0.45 MPa (minimum allowable pressure at the CCWS-1 circuit [6]) is 147.9ºC, which means that cavitation is not expected to happen for a beam power of 1.08 MW. It is important to mention that the current ITER CCWS-1 cooling layout proposes to connect two MB mirrors in series so that the inlet temperature would be 39.9ºC for the second mirror (temperature increase of 5.9ºC). Even with this higher temperature input, all the conclusions extracted from this analysis in terms of allowable pressure drop and acceptable temperature distribution remain valid.

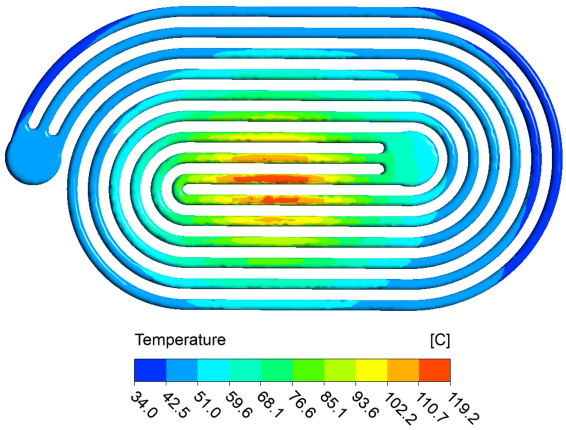

Fig. 9. Temperature distribution in the MB mirror cooling (reflecting side view)

3.2.3 Comparison among different beam deviations

The fluid-dynamic analysis described in section 3.1 was repeated to assess the thermal performance dependency of the MB mirror to different beam deviations. For this purpose, the heat flux distribution on the MB mirror reflecting surface obtained from the FALCON tests (Fig. 6) was mirrored according to two axes contained on the reflecting surface plane (Fig. 10).

The results from these simulations show that, although the temperature peaks are located according to the different beam center positions, the temperature distribution obtained for all the cases produces very similar peak values (Fig. 11). These results show that the current design of the MB mirror provides a good cooling performance with large temperature margins independent of the deviation direction of the incident beam.

4. Thermo-mechanical analysis

A steady-state thermo-mechanical analysis is performed in ANSYS Workbench 2021 R2 Static Structural [5] to assess ECH MB mirror in terms of plastic collapse and ratchetting against the loads taking place during the mm-wave normal operation for the upgraded power value of 1.08 MW [6]. This analysis provides the stress distribution, which is post-processed and subsequently compared with the allowable design limits available in the fabrication codes.

4.1 Model description

4.1.1 Geometry and mesh

This simulation covers, in addition to the MB mirror, the MB body, the bolting (bolts, washers and inserts), and metallic seals. Other components such as the leak monitoring ports, inlet and outlet cooling pipes at the MB body were removed from the assembly (the cooling pipes at the MB mirror were kept).

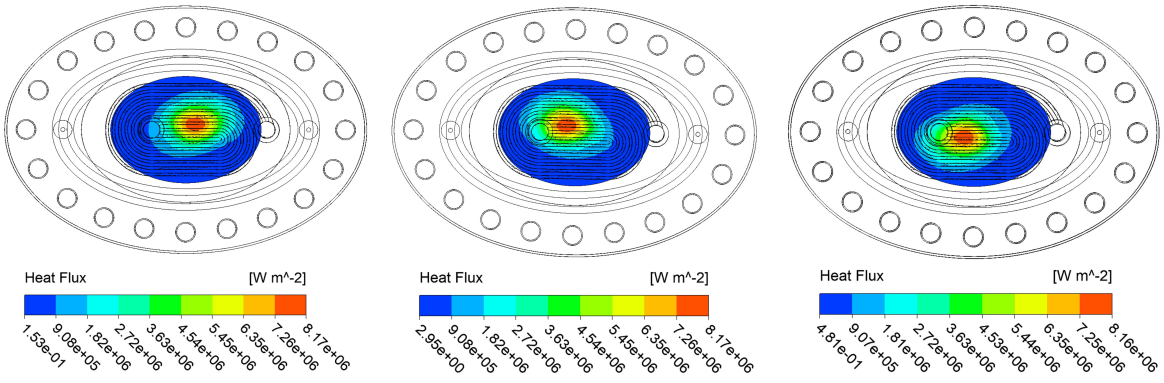

Fig. 10. Comparison among the applied beam losses on the MB mirror reflecting surface (non-reflecting side view)

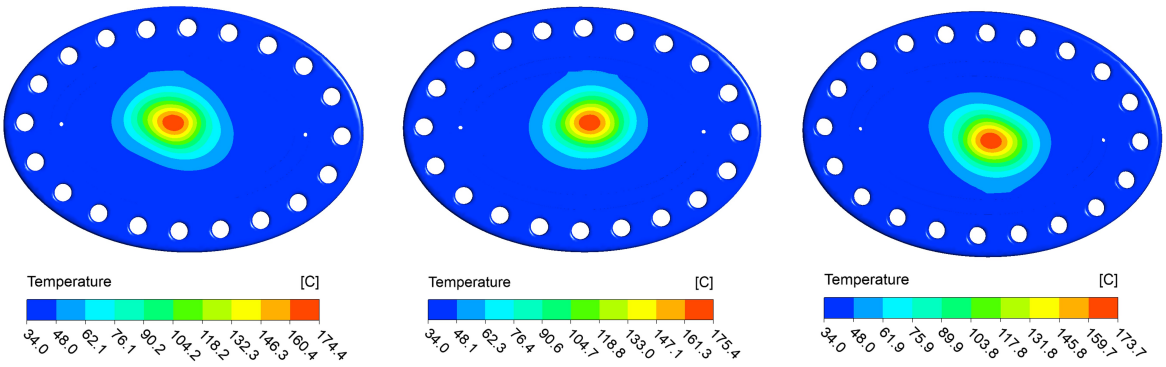

Fig. 11. Comparison among the temperature distributions in the MB mirror (reflecting side view)

The two metallic seals (Fig. 12) were modelled as prismatic rings with rectangular cross sections of 1 mm width (estimated contact surface after compression) and 2.6 mm height (seal cross section diameter before compression). An initial separation between faces (0.47 mm, seal compression recommended by the supplier) was defined as the starting state of the model to properly simulate the bolt pretension process.

Uniform mesh size values of 1.5 mm, 3 mm and 6 mm were applied to the MB mirror (both MB mirror and MB mirror cap), bolting and MB body, respectively. The total number of nodes and elements for the entire model are 1620737 and 1113042, respectively.

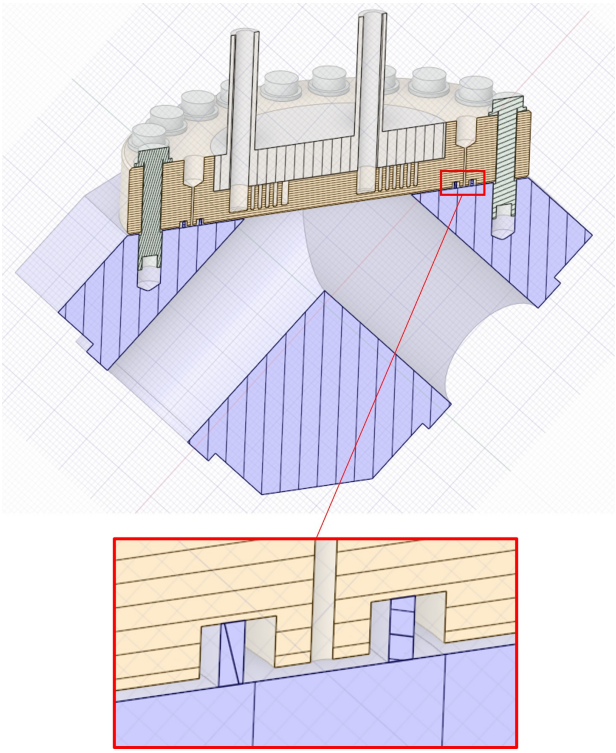

Fig. 12. Cross-section of the geometrical model used in the thermo-mechanical analysis

4.1.2 Material properties

The material properties related to the CuCr1Zr alloy, stainless steel 316L(N)-IG and Inconel 718 are extracted from the ITER Materials Properties Handbook [8] and applied to both MB mirror and MB body, MB mirror cap and bolting, respectively. These properties are introduced in the model as temperature-dependent table of values. The material behavior for these materials is considered as elastic.

The modelling of the metallic seals is carried out following the methodology developed in [9]. The complex behaviour of the metallic seals is simulated by introducing their non-linear hysteresis force-deformation curves.

3.1.3. Boundary conditions and loads

The thermo-mechanical analysis of the MB mirror is divided in three different time steps for the load application (Table 1).

Table 1. Load steps

Load step	Pre-tension (each bolt)	Cooling pressure	Temperature distribution
1	18 kN	-	-
2	Lock	1 MPa	-
3	Lock	1 MPa	Fig. 8

In the first load step, a pretension value of 18 kN is applied in the bolts defining the coupling between the MB mirror and the MB body to properly compress the double metallic seal and maintain the leak tightness throughout the ITER lifetime. A uniform pressure value 1 MPa [6] is applied in the second load step on the MB mirror surfaces in direct contact with the cooling water. Finally, the temperature distribution obtained in the fluid-dynamic analysis of the MB mirror (Fig. 8) was imported and applied in the second load step as an input in the thermo-mechanical simulation. A uniform temperature of 34°C (CCWS-1 inlet temperature [6]) was imposed to the components that were not included in fluid-dynamic analysis of the MB mirror, such as the MB body, the bolting, or the metallic seals.

4.2 Results

4.2.1 Code assessment

The design-by-analysis rules prescribed in RCC-MRx [10] are considered for the design validation of the MB mirrors. These components are classified as class N1Rx in the RCC-MRx code (highest safety classification), so these are subjected to the rules defined in Subsection B. The elastic analysis approach is selected for the assessment of plastic collapse (P-type damage) and ratcheting (S-type damage) failures modes. In this method the stresses are computed using an elastic analysis and classified into categories for their comparison with the allowable limits.

This stress categorization is performed by linearizing the stress (membrane, bending and peak) along the so-called Supporting Line Segment (SLSs). Outside the discontinuity areas, the SLS is the line segment perpendicular to the median surface of the wall. In discontinuity zones, the SLS is the shortest segment which joins the two sides of the wall.

The following criteria shall be satisfied to evaluate the protection against plastic collapse and ratcheting:

$$\overline{P_m} \leq S_m(\theta_m) \quad (3)$$

$$\overline{P_L} \leq 1.5 \cdot S_m(\theta_m) \quad (4)$$

$$\overline{P_L + P_b} \leq 1.5 \cdot S_m(\theta_m) \quad (5)$$

$$\mathrm{Max}(\overline{\mathrm{P_L} + \mathrm{P_b}}) + \overline{\Delta \mathrm{Q}} \leq 3 \cdot \mathrm{S_m}(\theta_\mathrm{m}) \quad (6)$$

Where $\overline{\mathrm{P_m}}$ is the general primary membrane intensity, $\overline{P_L}$ is the general local membrane intensity, $\overline{P_L + P_b}$ is the primary membrane plus bending stress intensity, $\mathrm{Max}(\overline{\mathrm{P_L} + \mathrm{P_b}})$ is the sum of the maximum stress value, $\overline{\Delta \mathrm{Q}}$ is the secondary stress range value and $\mathrm{S_m}(\theta_\mathrm{m})$ is the allowable stress for the temperature θ_m.

The most stressed cross-section of the MB mirror occurs at the beam center due to the temperature gradient existing at this location (Fig. 13). A set of 15 SLSs are defined on this cross-section for each cooling channel covering the 3 mm thickness of the reflecting surface (Fig. 14). Table 2 and Table 3 report the categorized stresses for each SLS and their comparison with the allowable limits. The four criteria previously described are fulfilled for all the SLS. The most compromised SLS is SLS9 (beam center location) for criterium (6) with a usage factor of 0.28. Regarding criteria (3) and (5) (criterium (4) is enveloped by criterium (3)), the most compromised SLS is SLS1 with usage factors of 0.67 and 0.68, respectively.

Stress peaks also appear at the locations in contact with the washers as a result of the large pretension applied in the bolts. However, these stress values do not jeopardize the mechanical integrity of the MB mirror because of the much thicker cross-section at these locations.

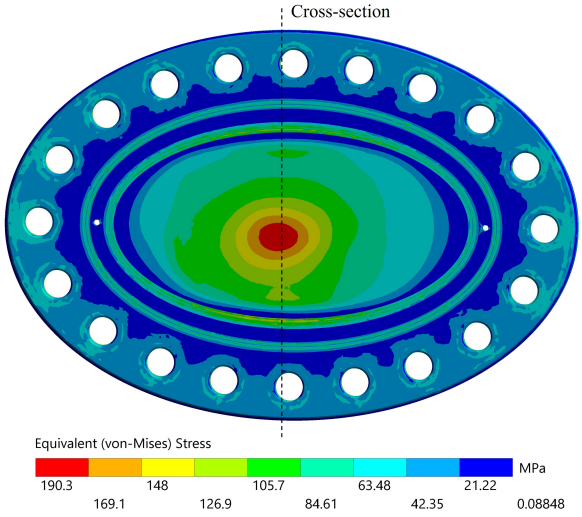

Fig. 13. Von-Mises stress distribution in the MB mirror (reflecting side view)

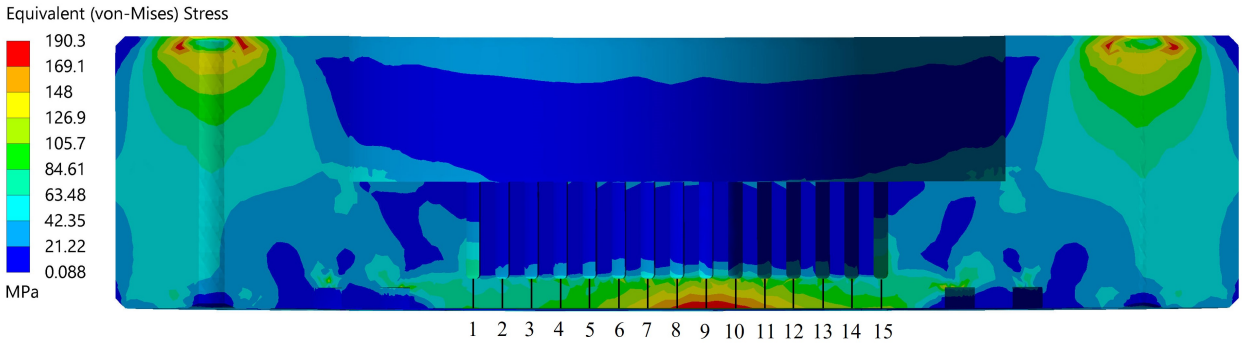

Fig. 14. SLSs for stress verification on the MB mirror

Table 2. MB mirror stress verification, values in MPa (SLS 1-8)

SCL	1	2	3	4	5	6	7	8	Limit
$\overline{\mathrm{P_m}}$	28.8	24.7	24.6	24.1	24.4	26.1	25.9	24.5	86
P_L	-	-	-	-	-	-	-	-	129
$\overline{P_L + P_b}$	40.8	27.9	30.7	33.0	36.1	38.7	37.0	36.4	129
$\mathrm{Max}(\overline{\mathrm{P_L} + \mathrm{P_b}}) + \overline{\Delta \mathrm{Q}}$	80.7	76.7	76.5	84.2	94.8	115.3	143.6	165.9	258

Table 3. MB mirror stress verification, values in MPa (SLS 9-15)

SCL	9	10	11	12	13	14	15	Limit
$\overline{\mathrm{P_m}}$	25.5	25.4	24.6	24.4	24.3	24.6	26.6	86
P_L	-	-	-	-	-	-	-	129
$\overline{P_L + P_b}$	35.0	34.8	33.4	30.9	27.5	27.4	39.4	129
$\mathrm{Max}(\overline{\mathrm{P_L} + \mathrm{P_b}}) + \overline{\Delta \mathrm{Q}}$	183.7	175.3	151.5	129.4	111.7	99.9	100.5	258

4.2.2 Reflecting surface deformation

The deformation of the MB mirror reflecting surface shall be minimized to reduce the beam losses and the High Order Mode (HOM) conversion during the mm-wave power transmission.

Fig. 15 shows the reflecting surface deformation according to the Z axis (local coordinate system with the XY plane contained on the initial reflecting surface). After the bolt tightening process, the MB mirror reflecting side acquires a slightly concave shape, due to the local bending moment generated by the bolts and metallic seals reactions. Once the temperature distribution is applied, the reflecting surface expands to a larger extent than the non-reflecting side of the MB mirror (due to the larger temperature values), which causes the mirror reflecting side tends to acquire a convex shape (Fig. 16).

The maximum deformation values take place at the beam center, reaching a value of up to 0.016 mm. The minimum deformation values appear at the transition between MB mirror edge and the central bump, reaching a minimum value of -0.032 mm. The maximum MB mirror deflection is 48 μm, estimated from the previously mentioned maximum and minimum deformations values. The mode conversion for this deflection value can be estimated as 0.24%, which is smaller than the mode conversion in an ideal miter bend with a flat mirror (0.37%) [11].

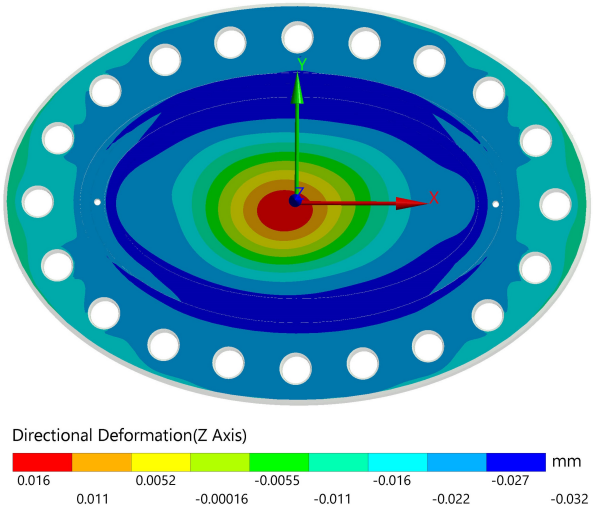

Fig. 15. Local deformation of the MB mirror (reflecting side view)

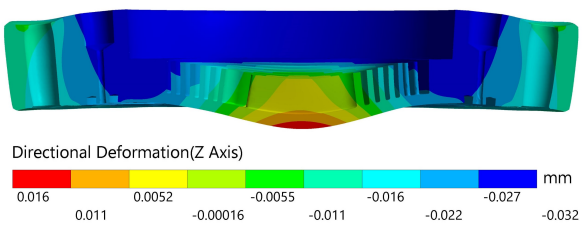

Fig. 16. Local deformation of the MB mirror (cross-section, amplification factor 200)

4.2.3 Seal compression

The proper compression of the metallic seals shall be assured, not only after the tightening process, but during the entire component lifetime, to guarantee the confinement of the primary vacuum. According to the supplier [9], the confinement can be guaranteed if the seal decompression is lower than one third the elastic recovery of the metallic seal (spring back), which in this case is 0.085 mm; so, one third is 0.028 mm for both metallic seals.

After the bolt tightening process, the target compression value of 0.47 mm cannot be completely achieved due to the MB mirror bending, reaching a maximum compression value 0.4637 mm in the larger seal (Fig. 17). The values obtained after the application of the full set of loads are very similar to the ones previously mentioned, which means that the coupling design can properly take the MB mirror deformations during mm-wave operation (Fig. 18).

Using a conservative approach we take the highest compression value after the tightening process (0.4637 mm, Fig. 17) and the lowest one after all the loads are applied (0.4589 mm, Fig. 18). The difference between these two values is 0.0048 mm, which is a conservative value of the seal decompression, as this value is much smaller than 0.028 mm. Therefore, the confinement of the primary vacuum during normal operation is assured.

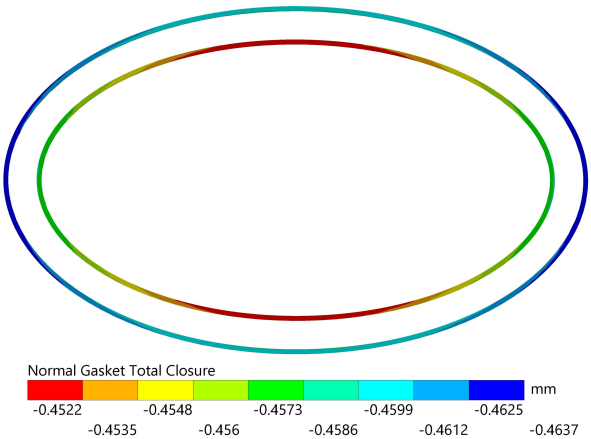

Fig. 17. Double metallic seal compression after the bolt tightening process

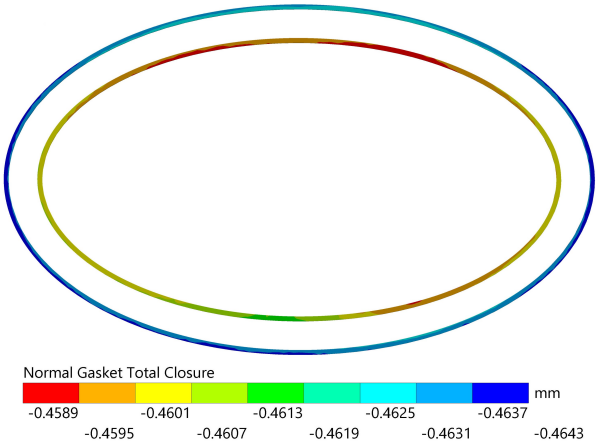

Fig. 18. Double metallic seal compression after the full set of loads

5. Conclusions

A new MB mirror cooling concept consisting of a spiral-shaped circuit with three channels in parallel was proposed to better dissipate the deposited power during the mm-wave normal operation. The off-centered beam configuration was used in the analyses since this distribution provides more demanding peak heat flux values in comparison with the theoretical function representing a perfectly-centered beam. This is a conservative approach since the expected temperature is higher yielding higher surface resistance and thus even higher temperatures than the perfectly-centered case.

The fluid-dynamic analysis showed that the power deposited on the MB mirror reflecting surface can be properly removed with a mass flow rate of 0.15 kg/s, resulting in an admissible pressure drop and acceptable flow velocity values in the cooling water. The maximum temperature for the MB mirror appears on the mirror surface at the beam center, reaching a value of 174.6ºC.

Regarding the MB mirror cooling water, the maximum local temperature occurs at the region close to the reflecting surface, reaching 119.2ºC, which is lower than the boiling temperature, even at the lowest allowable working pressure. The results from the analyses considering different beam deviation directions produced temperature distributions with very similar values, showing that this design is able to provide a good cooling performance independent of the deviation of the incident beam.

The comparison between the categorized stresses obtained from the thermo-mechanical analysis and the allowable design limits according to RCC-MRx show that the MB mirror design is widely capable of withstanding (in terms of the plastic collapse and ratcheting) the expected loads taking place during the normal mm-wave operation scenario. The MB mirror reflecting surface experiences a maximum deflection of 48 μm, which is equivalent to only 0.24% mode conversion. The seal decompression values obtained in the simulation are much smaller than the maximum value recommended by the supplier, assuring that the confinement of the primary vacuum is maintained during the mm-wave operation.

Acknowledgments

This work was supported in part by the Swiss National Science Foundation. This work was carried out within the framework of the F4E contract F4E-OFC-0958. The views and opinions expressed herein do not necessarily reflect those of the European Commission or the ITER Organization.

References

[1] D. Strauss, et al., Nearing final design of the ITER EC H&CD Upper Launcher, Fusion Eng. Des. 146, Part A (2019) 23-26

[2] P. Santos, et al., Thermal mechanical analyses of the mm-wave miter bend for the ITER electron cyclotron upper launcher first confinement system, Fusion Eng. Des. 136, Part A (2018) 650-654

[3] A. Mas Sánchez, et al., Numerical analyses of the Monoblock Mitre Bend for the ITER Electron Cyclotron Upper Launcher, Fusion Eng. Des. 165 (2021) 112212

[4] A. Xydou, et al., Prototype mitre bends of the ex-vessel waveguide system for the ITER upper launcher: Thermal hydraulic simulations and experiments with off-center mm-wave beams, Fusion Eng. Des. 170 (2021) 112457

[5] http://www.ansys.com/

[6] N. Casal, et al., EC UL/EW Load Specification, ITER_D_653WG8 v3.6 (2021)

[7] T. Goodman, et al., ECH UL millimeter transmission line components thermal loading, F4E_D_2PQ5GS v1.1 (2022)

[8] J. Campbell, et al, ITER Material Properties handbook properties, ITER_D_2239QQ v1.0 (2005)

[9] A. Mas Sánchez, et al., Mechanical analyses of the waveguide flange coupling for the first confinement system of the ITER electron cyclotron upper launcher, Fusion Eng. Des. 109-111, Part A, (2016) 532-538

[10] RCC-MRx Code, Section III, Tome 1, Subsection B, Class 1 N1Rx Reactor Components its Auxiliary Systems and Support (2018)

[11] J. Doane, et al, Power monitor miter bends for high-power microwave transmission, Fusion Engineering and Design 93 (2015) 1–8